OUKA
The University of Osaka
Institutional Knowledge Archive

Title	Some Fundamental Properties of High Power CO_2 Laser Beam as a Heat Source
Author(s)	Arata, Yoshiaki; Miyamoto, Isamu
Citation	Transactions of JWRI. 1974, 3(1), p. 1-20
Version Type	VoR
URL	https://doi.org/10.18910/3813
rights	
Note	

The University of Osaka Institutional Knowledge Archive : OUKA

https://ir.library.osaka-u.ac.jp/

The University of Osaka

Some Fundamental Properties of High Power CO_2 Laser Beam as a Heat Source†

Yoshiaki ARATA* and Isamu MIYAMOTO**

Abstract

The interaction between the metallic material and focused CO_2 laser beam with power level of several hundred watts is studied. The energy density distribution of the focused CO_2 laser used in this experiment can be approximated by a Gaussian curve with a diameter of 0.5 mm at e^{-1} power point. The beam absorptance of polished metal is low and only about 10 % at most, in proportion to square root of dc specific resitivity of metal. A weldability of metal by CO_2 laser is proportional to $ak^{3/2}\theta_f$ under the polished surface condition, and is to $ak\theta_f$ under the condition of the 100 % absorptance. The interaction between the focused laser beam and metallic specimen with various surface conditions based on measurements of the beam absorptance and the temperature, observation by means of high speed camera and analysis of heat conduction. As a results, it was found that in order to enhance the beam absortance the surface treatment was effective.

The effect of the surface treatment on the beam absorptance becomes larger with lower melting point θ_f of and higher thermal conductivity k of the metal and higher boiling point of the treated surface layer, and under such a condition the absorptance is almost the same in different surface treatments. Examples laser-processed are shown.

1. Introduction

Since laser is coherent beam with excellent monocromaticity and directivity, a small and high density spot can be readily obtained through a simple optical system. Solid state lasers such as ruby, the glass and YAG, and CO_2 gas laser are used as a processing heat source. The former is suitable for special processing like drilling and spot welding because its power output its pulsive with extremely high peak power. As the lattes has CW high power as well as high efficiency, it can cover a wide range of continuous processing containing welding, cutting and drilling.

Compared to the electron beam which is the existing high energy density source, laser has a low efficiency, and even CO_2 laser has 10～20 % efficiency at most, but has the advantages of no X-ray emission, no need of vacuum chamber, and easy control of beam.

In this paper, the comprehensive properties of CO_2 laser as a heat source mainly for metallic materials are discussed based on the theoretical and experimental analysis of the interaction between focused CO_2 laser beam and materials.

In general, under irradiation of an extremely high energy density beam more than about 10^5 W/cm^2, the mechanical force acompanied with violent vaporization depresses the metal fused and makes a hole where the beam is effectively trapped. On the other hand, below about 10^5 W/cm^2, the beam acts upon the metal as a surface heat source and drilling phenomenon scarcely appears, of which case is dealt with here.

This paper consists of eight sections. Section 2 shows the CO_2 laser apparatus used in this experiment and the properties of the laser beam and section 3 gives the optical system and the energy density distribution in a focal spot. Section 4 developes the theory on thermal conduction in laser heating of sheet metal, and section 5 discusses the optical properties of the metallic material for CO_2 laser beam, and its weldability. Section 6 shows the interaction between a focused laser beam and materials i. e. metallic material with different surface conditions, and non-metallic materials. Section 7 explains the processing methods for welding and cutting and some examples of cuts and welds, and section 8 summarizes the conclusions of this study.

2. CO_2 Laser Apparatus

Figure 1 shows a schematic diagram of the CO_2

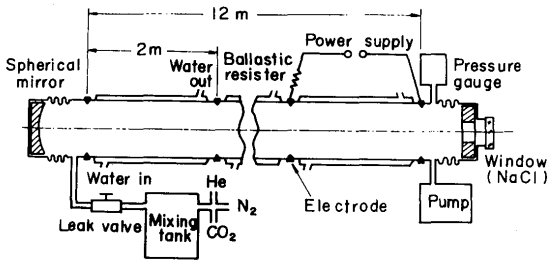

Fig. 1. Schematic diagram of 12m CO_2 laser.

† Received on Aug. 6, 1973

* Professor

** Research Instructor, Dept. of Welding Engineering, Faculty of Engineering, Osaka University

laser used in this experiment. It consists of a water-cooled discharge tube 74 mm i. d., 12 m long, placed between gold evaporated plane and 29.2 m radius curvature mirrors. The laser power with a wavelength 10.6 μ was coupled out from the cavity through a 15 mm diam hole at the center of the plane mirror. There are six sections to the tube, each section with 2 m long having its own cathode with a ballast resistor. A cold cathode discharge, either ac or dc, was run on each section in a flowing gas mixture of CO_2, N_2 and He with very slow mass flow rate.

The measurements of the laser power level were carried out with the power meter shown in **Fig. 2.** Water flows through the power meter at a constant rate which is monitored by a flow meter, and the temperature difference of input and output water is measured by a pair of thermisters which makes the temperature measurements very precise. Then a detecting voltage of the bridge, V_b, is recorded on charts. To make the measurements accurate, a heater is incorporated for calibrating the V_b-value with an electrical input of known power level. The absorption plate of the power meter consists of a thin aluminum plate anodized uniformly, and its absorptance was measured by 100 % absorptance power meter[1]. A response time of this power meter was shorter than 1 second.

In this experiment, the laser was operated mainly from 60 Hz electric power supply which gave a pulsed output of 120 Hz. The waveform measured by a Au-doped germanium is shown in **Photo. 1.**

Maximum output power level about 500 W was obtained under condition mixing ratio of gas mixture (10 torr) was $CO_2 : N_2 : He = 1 : 5 : 40$, and discharge current and voltage to each tube were about 100 mA and 7.8 KV respectively.

The divergent angle of the laser beam was measured by a simple method; a film was placed in a plane vertical to the laser beam at a given distance from the laser head, and was heated by the laser beam for a given time. The diameter of the scorched area in the film was measured. **Figure 3** shows the relation between the diameter of the scorched spot

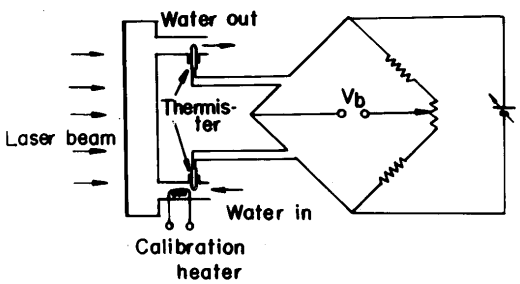

Fig. 2. Schematic diagram of power meter.

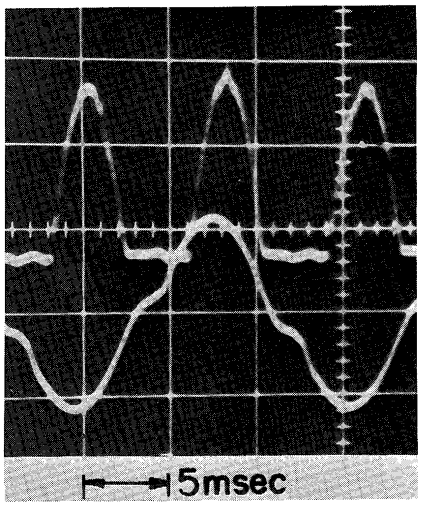

Photo. 1. Power output waveform detected with Au-doped Ge (upper) and Discharge current waveform (lower).

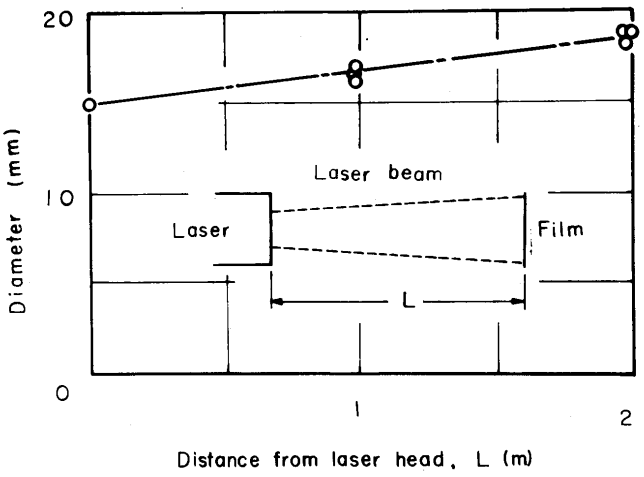

Fig. 3. Oscillated beam diameter vs distance from laser head.

and the distance from the laser head to the film L. The divergent angle obtained from this figure was about 1.8×10^{-3} radians.

3. Optical System

A CO_2 laser beam can be converged through a converging lens or concave mirror. In this test a metallic concave spherical mirror coated with vacuum deposited gold, with a radius 310 mm, was used in combination with a metallic plane mirror in order to converge the laser beam downward on a horizontal plane, as shown in **Fig. 4.**

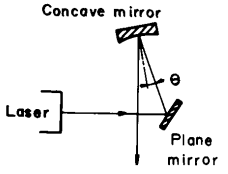

Fig. 4. Optical system to converge CO_2 laser beam. Radius of curvature of concave spherical mirror is 310 mm.

When a beam is converged through a concave spherical mirror, an angle θ between incident beam and the mirror axis cannot be zero, and astigmatism becomes a problem. In order to estimate the affect of the astigmatism, a thin film was irradiated by the beam focused through the optical system shown in Fig. 4, and an area of scorched spot was measured for the various incident angles as a function of the distance from the concave spherical mirror along the chief ray. In the series of this measurements, the laser power level and the irradiation time were kept at 40 W and 20 msec respectively.

Figure 5 shows the minimum spot area for each incident angle θ plotted as a function of θ. It was almost constant for $\theta<6°$, but increased gradually with increasing θ for $\theta>6°$. In order to obtain small beam spot by means of this optical system, it is necessary to make θ less than 6° in which the astigmatism is negligible small.

This method measuring the beam spot size using film is practically convenient, but the data obtained by this method are not precise because the diameter is affected by the laser power, and its heating time. The precise spot size should be determined based on the energy distribution profile in the beam spot as described above.

Figure 6 is the schematic diagram for measuring the energy distribution in a focal spot. A slit with a small square hole (0.1 mm×0.1 mm) which consisted of four copper foils (0.2 mm in thickness) was moved in the horizontal plane. The beam energy passed through the slit was measured by means of a thermocouple and recorded in relation to the location in the beam spot. In order to protect the thermal oxidation, the top surface of the copper foil was polished smoothly and shielded with argon gas during laser heating. The thermocouple and the back surface of the slit were cooled by a fan.

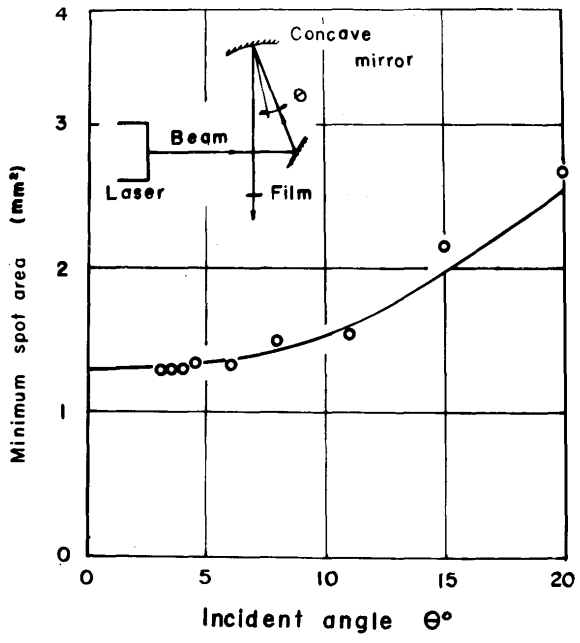

Fig. 5. Minimum spot area vs incident angle to the concave spherical mirror of radius 310 mm (beam diameter=15 mm).

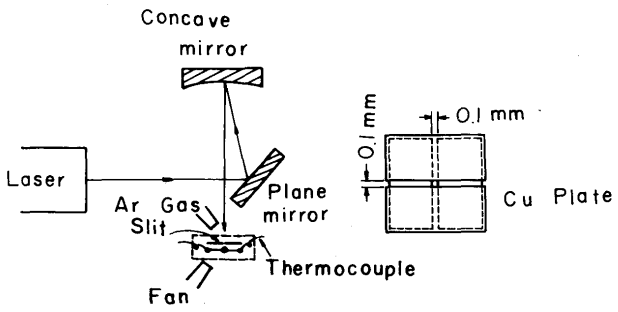

Fig. 6. (a) Experimental setup for measuring energy density distribution in focal spot.
(b) Detail of the slit.

In **Fig. 7** radial energy density profile measured is shown in comparison with the theoretical one calculated from a plane parallel beam with a wavelength 10.6 μ. The measured distribution profile may be well approximated by a Gaussian curve

$$w=\frac{W}{\pi a^2}\exp\left(-\frac{r^2}{a^2}\right) \quad \text{---------- (1)}$$

where r(mm) is the radial distance from the center and W is the laser power level. As shown in Fig. 7, a radius of 1/e power point was 0.25 mm, and was about four times as large as theoretical one. When

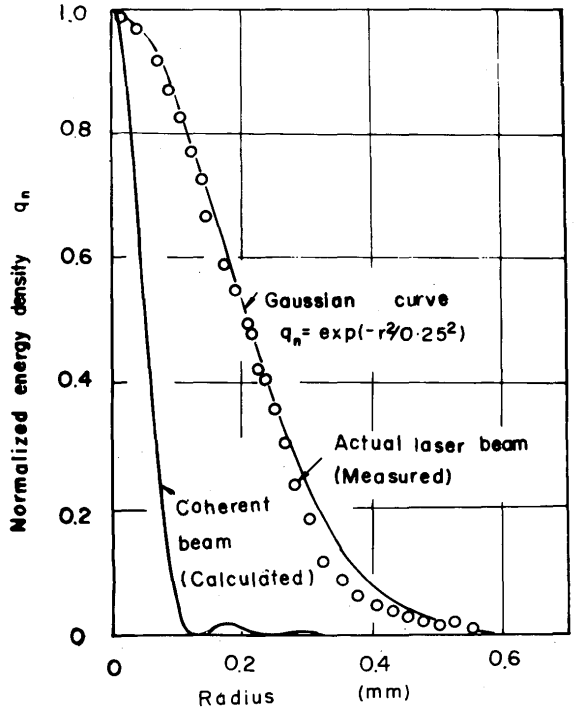

Fig. 7. Comparison between beam power density profile measured and one calculated from choerent beam (f=155 mm and beam diameter 15 mm).

the power level of laser is 100 W for example, the energy density at the center becomes about 5.6×10^4 W/cm^2.

4. Heat Conduction of Surface Heat Source

In analyzing the mechanism of heat processing such as welding, it is important to know the temperatures in the workpiece in relation to location, time and heating condition. Many researchers[2] have treated the actual heat source as a simplified model such as point or line. The treatments, however, are not enough to know precise temperature distribution, especially in the vicinity of the heat source.

In this section, the temperature distribution due to the surface source in which power varies with time, and power density is non-uniform is analyzed. In this analysis, the latent heat of fusion, heat losses through the surface to surrounding atomsophere, variation of the physical coefficients of material and the convection in the molten metal are neglected.

Then assuming that heat is liberated on the bounding plane of semi-infinite solid at the rate $W(t')\times q(x', y')\,dx'dy'$ per unit time at time t' in the element of small area $dx'dy'$ at point $(x', y', 0)$, the temperature rise at (x, y, z) at time t due to heat delivered from time zero to t is given by

$$\theta(x, y, z; t)=\frac{2}{c\rho}\int_0^t W(t')dt'\iint_S q(x', y'; t')\times\frac{c\,e^{-\frac{\{(x-x')^2+(y-y')^2+z^2\}}{4k_D(t-t')}}}{\{4\pi k_D(t-t')\}^{3/2}}dx\,dy' \quad \text{----- (2)}$$

where k_D = thermal diffusivity of the material
c = special heat of the material
ρ = density of the material, and

$$\iint_S q(x', y'; t)\,dx'dy'=1 \quad \text{----------(3)}$$

When the steady heat with an uniform flux density of w_0 over a circular region of which center is at origin is liberated from time zero on the surface of a semi-infinite solid, the temperature rise at (r, z) at t is given by

$$\theta(x, z; t)=\frac{2w_0}{\pi k}\sqrt{k_D t}\int_0^{\varphi_0}\left(\text{ierfc}\,\frac{\sqrt{z^2+l_2^2}}{\sqrt{4k_D t}}-\text{ierfc}\,\frac{\sqrt{z^2+l_1^2}}{\sqrt{4k_D t}}\right)d\varphi \quad \text{---------- (4)}$$

where $x^2+y^2=r^2$,

$$|l_1|=r\cdot\cos\varphi+(a^2-r^2\cdot\sin^2\varphi)^{1/2},$$

$$\text{ierfc}\,X=\int_X^\infty \text{erfc}\,u\cdot du$$

$$=\exp(-X^2)/\sqrt{\pi}-X\cdot\text{erfc}\,X,$$

and φ_0 and $|l_2|$ is given by

$$\varphi_0=\sin^{-1}a/r$$

$$|l_2|=r\cdot\cos\varphi-(a^2-r^2\sin^2\varphi)^{1/2},\ \text{when } r>a$$

$$\varphi_0=\pi$$

$$l_2=0,\ \text{when } r<a.$$

The steady temperature at origin is given by

$$\theta_m=\frac{aw_0}{k}=\frac{W}{a\pi k} \quad \text{----------(5)}$$

where $W=\pi a^2 w_0$.

For the source having the Gaussian energy density distribution

$$w(r)=\frac{W}{\pi a^2}\exp\left(-\frac{r^2}{a^2}\right), \quad \text{----------(6)}$$

the temperature rise on the z-axis is given in non-dimensional form as follows:

$$\theta^*(0, z^*; t^*)=\frac{1}{\sqrt{\pi}}\int_0^{t^*}\frac{\exp(-z^{*2}/\tau^{*2})}{1+\tau^{*2}}d\tau^* \quad \text{-------(7)}$$

where $l^*=l/a$ (l is quantity with a dimension of length)

$t^*=(2/a)\sqrt{k_D t}$ and

$\theta^*=\theta/\theta_m$

At the origin, it becomes

$$\theta^*(0, 0; t^*)=\frac{1}{\pi}\tan^{-1}t^* \quad \text{----------(8)}$$

Figure 8 shows the relationship between z^* and $\theta^*(0, z^*; t^*)$ for various values of t^*.

When the power $W(t)$ of the Gaussian source varies with time giving the energy density at time t as follows:

$$w(r, t)=\frac{W(t)}{\pi a^2}\exp\left(-\frac{r^2}{a^2}\right) \quad \text{----------(9)}$$

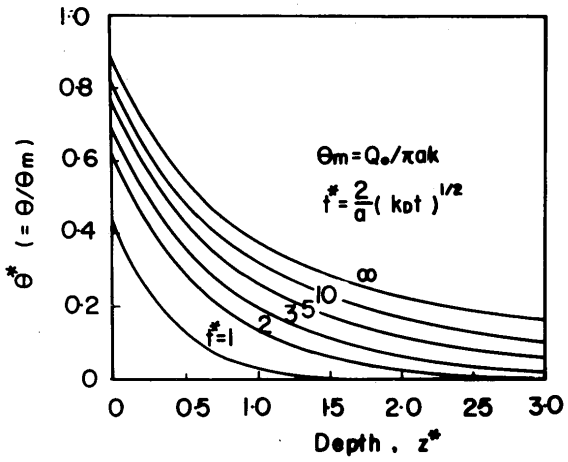

Fig. 8. Relationship between $z^*(=z/a)$ and $\theta^*(=\theta\pi ak/w)$ for semi-infinite solid (Gaussian source, $r^*=0$).

the temperature rise at origin at time t is written by

$$\theta(0,\,0\,;\,t)=\frac{a^2}{c\rho}\int_0^t\frac{W(t-t')\exp\{-z^2/4k_D(t-t')\}}{\sqrt{4\pi k_D(t-t')}\{4k_D(t-t')+a^2\}^{3/2}}\,dt' \quad \text{---------- (10)}$$

When the heat source moves at velocity v, the temperature rises at $(x,\,y,\,z)$ in the coordinates attached to the center of the source in quasi-stationary state is given by

$$\theta(r,\,z)=\frac{w_0}{\pi k}\int_0^{\pi}\int_0^{a}\frac{l}{R}\cdot\exp\left[-\frac{v}{2k_D}\,(R+r\cdot\cos\varphi-r'\cdot\cos\varphi')\right]\cdot r'\cdot dr'\cdot d\varphi'$$

for the circular source, and ---------- (11)

$$\theta(r,\,z)=\frac{q_0}{k\pi}\int_0^{\pi}\int_0^{\infty}\frac{1}{R}\cdot\exp\left[-\frac{v}{2k_D}\cdot(R+r\cdot\cos\varphi-r'\cdot\cos\varphi')-\frac{r^2}{a^2}\right]\cdot r'\cdot dr'\cdot d\varphi',$$

for the Gaussian sorvrce, ---------- (12)

where

$$R=[r'^2+r^2-2\cdot r'\cdot r\cdot\cos(\varphi-\varphi')+z^2]^{1/2}$$

Figures 9~11 show examples of isothermal lines in both traverse and longitudinal cross sections computed in cases of ideal point, circular and Gaussian source in quasi-steady state under conditions $d^*=1.2$ and $v^*=0.25$.

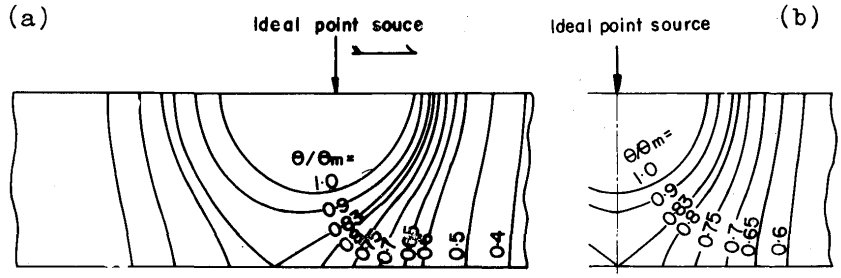

Fig. 9. Isothemal lines for ideal point source in quasi-steady state for d*=1.2 and $v^*=0.25$ (d=thickness of the plate).
(a) Longitudinal cross section (b) Transverse cross section (maximum value)

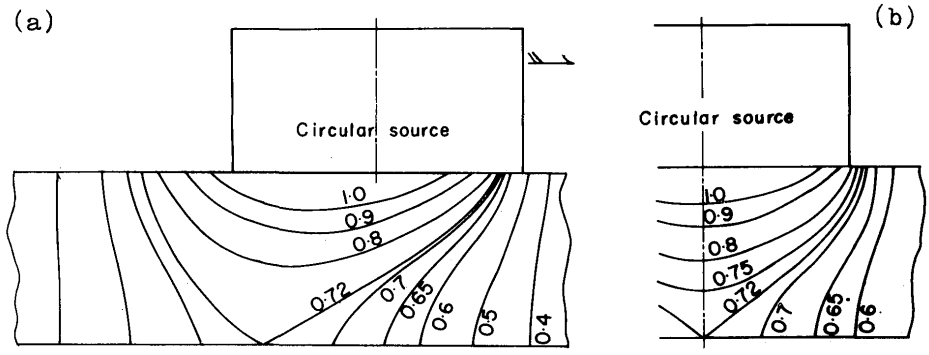

Fig. 10. Isothermal lines for circular source in quasi-steady state for d*=1.2 and $v^*=0.25$.
(a) Longitudinal cross section (b) Transverse cross section (maximum value)

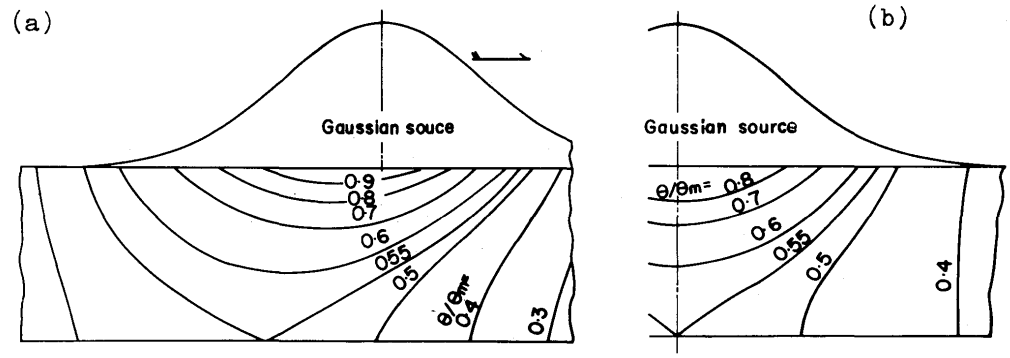

Fig. 11. Isothermal lines for Gaussian source in quasi-steady state for d*=1.2 and $v^*=0.25$.
(a) Longitudinal cross section (b) Transverse cross section (maximum value)

5. Optical Properties of Metal at Wavelength 10.6 μ

(1) Introduction

When a CO_2 laser is used for heat processing of metal such as welding, it is important to know the beam absorptance of the work piece, because a condition of the processing depends upon the absorptance. In general, the infrared absorptance of metal with smooth surface is very low, and is roughly proportional to the square root of the dc resistivity of the metal. Many workers[3] have measured the absorptance in the extreme condition, namely the absorptance of metal in highly polished, clear and stress-free surface condition or of evaporated metal film on the super smooth surface in high vacuum. In practice, however, the absorptance in the surface condition supplied by commercial vender or of various surface finished is necessary rather than the extreme condition described above, but these measurements have not yet been undertaken.

In this section, the experimental data of the absorptance of metal in the surface condition supplies by commercial vender are shown in comparison with the values obtained from the electro-magnetic theory, and a "CO_2 laser weldability" of various metals is estimated on the basis of this optical property of metal in combination with heat conduction theory.

When metal is heated by several kilo-watts laser or higher, molten metal produced around heated position is often depressed by vaporization of metal, so that a deep hole, which traps the beam effectively, is formed. Then the absorptance increases, sometimes up to near 100 %, and it does not almost depend upon the optical properties of metal. Here, the absorptance in such a situation is not dealt with.

(2) Optical Properties of Metal

The two most characteristic optical properties of metal are the opacity and the high reflecting power of its polished surface. One valence electron in metal which interacts with the light is equivalent to the system containing a free electron with the effective mass m^* and some of harmonic oscillators with a given specific frequency, but in the infrared the absorptance of metal is dominated by conduction absorptance due to free electron.

It is well known that for the electromagnetic wave with the frequency ω_0 electric permitivity of metal may be obtained by replacing that of insulater $\varepsilon(\varepsilon_0$ in vacuum space) having real quantity with a complex quantity $\tilde{\varepsilon}$;

$$\left.\begin{aligned} \varepsilon &= \varepsilon + i\frac{\sigma}{\omega} \\ \text{or}\quad \varepsilon^* &= \varepsilon^* + i\frac{\sigma}{\omega\varepsilon_0} = \varepsilon^* + i\sigma^*, \end{aligned}\right\} \qquad (13)$$

where σ is the electrical conductivity of metal, setting $\varepsilon = \varepsilon_0 \cdot \varepsilon^*$, ε^* is dielectric constant and dimensionless parameter. And then the optical constants, n and k, are illustrated in terms of the electric parameters, ε^* and $\varepsilon^*(\equiv 1/\eta^*)$;

$$\left.\begin{aligned} k &= -\varepsilon^*\eta^* + [\varepsilon^{*2}\eta^{*2}]^{1/2} \\ n^2k^2 &= \frac{1}{2}\{-\varepsilon^* + [\varepsilon^{*2} + \sigma^{*2}]^{1/2}\} \end{aligned}\right\} \qquad (14)$$

The reflectance at surface with complete smoothness of metal in the case of the normal incident is given by Fresnel's equation,

$$\begin{aligned} R &= \left|\frac{\tilde{n}-1}{\tilde{n}+1}\right|^2 \\ &= \frac{(n-1)^2 + n^2k^2}{(n+1)^2 + n^2k^2}, \end{aligned} \qquad (15)$$

where $\tilde{n} = n(1+ik)$.

This may be obtained by substituting Eq. (14) into Eq. (15).

In general, since σ and σ^* (or η^*) are the function of ω, it should be obtained from the free electron theory of Drude. However, when the wavelength of light is sufficiently long, giving slowly varying electric field, the current in metal can be treated as being steady which is propertional to the electric field. If σ_0 or $\sigma_0^*(=\sigma_0/\omega\varepsilon_0)$, which is determined from experiments on stationary of slowly varying current, is used for σ or σ^* value corresponding to the infrared, for instance, for copper $\sigma_0 = 5.8\times10^7$ ohm^{-1} m^{-1} and taking $\omega = 1.78\times10^{14}$ sec^{-1} corresponding to the CO_2 laser beam, 10.6 μ, $\sigma_0^* = 37000$ may be obtained with $\varepsilon_0 = 8.85\times10^{-12}$ farad$\cdot$m^{-1}. A ε^* is of the order of unity and therefore is small compared with the σ_0^* value computed above. Therefore, Eq. (14) gives a good approximation;

$$\left.\begin{aligned} k &= 1 \qquad \text{(a)} \\ n^2 &= \frac{1}{2}\sigma_0^* \qquad \text{(b)} \end{aligned}\right\} \qquad (16)$$

Substituting Eq. (16) into Eq. (15), the infrared absorptance of metal may be written

$$\begin{aligned} A_b &= 1 - R \\ &= \frac{2}{n} = \sqrt{8\eta_0^*} \end{aligned} \qquad (17)$$

For CO_2 laser beam, Eq. (17) fields

$$A_b = 112.2\sqrt{\eta_0} \qquad (18)$$

where η_0 is dc resistivity of metal σ_0^{-1}. This is the well-known Hagen-Rubens's equation.

(3) Experimental Procedures

During measurement of the absorptance, output power of the CO_2 laser was monitored by the power meter shown in Fig. 2. The absorptance of metal at room temperature was obtained by measuring the absorbed power of an another power meter which was similar to one described above except that the absorption plate of the power meter was replaced by the specimen of thin metal with unknown absorptance. In this case, unfocused radiation beam, 15 mm in diameter, with power level of approximately 200 W was supplied to the specimen. A thin metal, 0.3 mm in thick, was used to reduce the temperature gradient within the specimen in direction of the thickness, and then its surface temperature was kept nearly at room temperature during measurement since its opposite surface was cooled with water.

Figure 12 shows a schematic diagram of the experimental setup for measuring the absorptance of molten metal. The molten pool was produced by the laser heating of the specimen using the beam focused through the optical system indicated in Fig. 4. The optical system was adjusted so as to have its focal point on the surface of the specimen. A shutter consists of a rectangular plate with a window which falls freely, and determins the beaming time. Each specimen heated by the laser was immediatly thrown into the calorimeter shown in **Fig. 13** and the calorimetric gain was measured. A heater and a thermister were incorporated to the system, and the similar circuit as shown in Fig. 2 was used; in this case one of the thermisters was replaced by a solid resister. The relation between electrical input to the heater, and change of V_b-value was checked beforehand, and thus in order to obtain the energy absorbed by the specimen, the V_b-value was recorded before and after the specimen was thrown in calorimeter. The absorbed energy, in calories, is plotted as a function of beaming time, and the absorptance may be computed from the incident laser energy, in calories, to the specimen and slope of a curve obtained from these experimental values.

(4) Absorptance of Polished Metal

In practical metal processing using CO_2 laser, the absorptance of metal in the surface condition supplied by a commercial vender is necessary rather than that in the extreme condition mentioned above. The sheet metal, 0.3 mm in thick was received in the from of highly polished strip, and was sheared into 3 cm×3 cm. Then the specimen was rinsed with a neutral detergent, and then with benzen. Though smoothness, purity, removal of residual stress and cleanliness of the specimen are not so good in comparison with other workers[3], the authors call these specimens "polished metal".

The absorptance of various metals for high power CO_2 laser beam was measured at both room and fusion temperatures using calorimeter. In **Fig. 14** the absorptance of polished metals at both temperatures is plotted vs square root of dc resistivity, in $(\mu\Omega\cdot cm)^{1/2}$ The experimental absorptance and theoretical one calculated from Eq. (18), which is shown by a solid

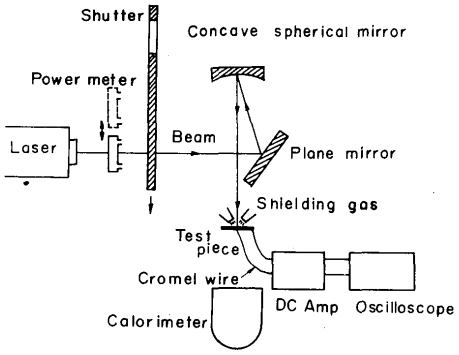

Fig. 12. Experimental setup for measuring the beam absorptance of the molten metal.

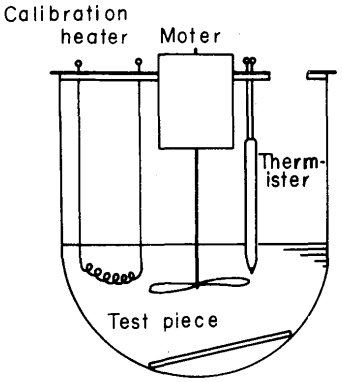

Fig. 13. Shematic diagram of carolimeter in Fig. 12.

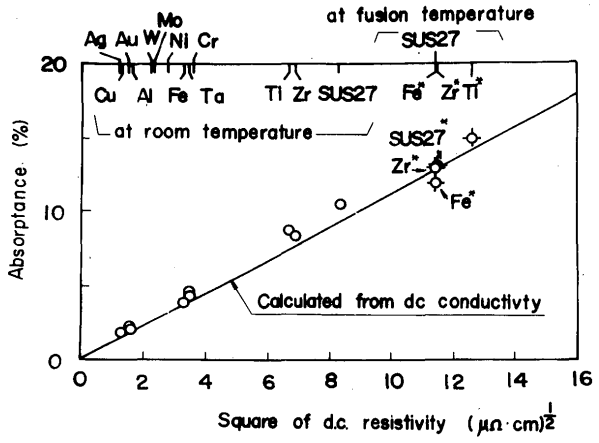

Fig. 14. Absorptance of a metal at room and fusion temperature. The data corresponding to fusion temperature are marked with symbol * and SUS27 standarized by JIS corresponds to AISI304 stainless steel.

line on this figure, are in reasonably good agreement at both temperatures. At room temperature, SUS27*) stainless steel has the highest absorptance and copper has the lowest one of any measured metal. At the fusion temperature the absorptance is large in comparison with one at the room temperature due to increase in the resistivity of metal, but it does not exceed 15 %, so that most incident laser energy is lost due to elect reflection.

(5) Laser-Weldability of Metals

When material is heated by focused CO_2 laser beam, its temperature rise depends upon the energy distribution profile and power level impinged as well as the beam absorptance and heat conduction properties of material. Therefore, it is useful to estimate the CO_2 laser-weldability of material in term of the minimum power level required to melt the material from its optical and heat conduction properties.

When focused CO_2 laser beam, having Gaussian flux distribution with radius a of $1/e$ intensity at center, impinges upon the surface of semi-infinite material, of which beam absorptance is A_b, temperature rise at location on the beam axis in steady state becomes, by Eq. (7), in simplified form:

$$\theta(O,\ z;\infty)=\frac{A_bQ_0}{2\sqrt{\pi k}}\ \exp(z^2/a^2)\cdot\mathrm{erfc}(z/a) \quad \text{-------(19)}$$

where Q_0 is the total laser power per unit time. At center of the source, (0, 0)

$$\theta(O,\ O;\infty)=\frac{A_bQ_0}{2\sqrt{\pi ka}}\doteqdot\frac{\sqrt{\pi}}{2}\ A\theta_m. \quad \text{----------(20)}$$

Minimum power required to melt surface of semi-infinite solid is given by

$$Q_f=\frac{2\sqrt{\pi}\,ka}{A_b}\,\theta_f \quad \text{----------(21)}$$

where θ_f is fusion temperature of material.

In the case of polished metal, the absorptance at fusion temperature is given by

$$A_f=4\sqrt{\frac{\pi c\varepsilon_0\eta_f}{\lambda}} \quad \text{----------(22)}$$

where c is velocity of light, ε_0 the electric permativity of vacuum, η_f dc resistivity of metal at fusion temperature and λ wavelength of the beam. Substitution of Eq. (22) into Eq. (21) yields

$$Q_f=\frac{1}{2}\ ka\sqrt{\frac{\lambda}{c\varepsilon_0\eta_f}}\ \theta_f \quad \text{----------(23)}$$

For CO_2 gas laser beam, $\lambda=10.6\ \mu$. With $c=3\times10^{10}$ cm/sec and $\varepsilon_0=8.85\times10^{-14}$ farad/cm, and taking $a=$ 0.025 cm, Eq. (23) gives

$$Q_f\cong3\times10^{-2}\ \frac{ak\theta_f}{\sqrt{\eta_f}} \quad \text{----------(24)}$$

If the absorptance of material is enhanced up to 100%, Eq. (21) yields

$$Q_f=2\sqrt{\pi}\,ka\theta_f \quad \text{----------(25)}$$

Assuming that law of Wiedermann-Franz, in which electrical conductivity of pure metal is proportional to its thermal conductivity, holds at fusion temperature, Eq. (24) for polished metal becomes

$$Q_f\propto ak^{2/3}\,\theta_f \quad \text{----------(26)}$$

In comparison with Eq. (25) for 100 % absorptance metal in which Q_f is proportional to $ak\theta_f$, affect of k on Q_f is large. **Figure 15** shows Q_f for various metals of semi-infinite thickness in both cases, polished and of 100 % absorptance. As it is clear from this figure, iron, zironium, titanium, SUS27 etc. may be relatively easily processed by CO_2 laser in polished surface condition: Q_f is about 200 W for titanium and SUS27 and 300—400 W for iron and zirconium. On the other hand both silver and copper in polished surface condition are most difficult: Q_f of both metals is extremely high value, 9—10 KW. Thus in polished surface condition, difference of Q_f in metal is large and comparatively higher laser power is required.

On the other hand, when the absorptance is enhanced up to 100 %, difference of Q_f in metal becomes small and the magnitude of Q_f falls to less than 300 W at most.

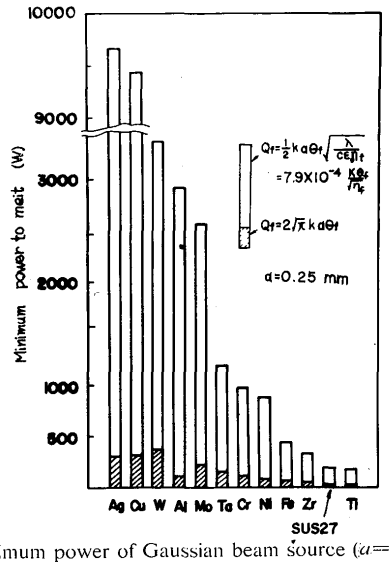

Fig. 15. Minimum power of Gaussian beam source (a=0.25 mm) for melting semi-infinite metal. Blank and hatched columns correspond to the value for polished and 100 % absorptance metals respectively.

*) The SUS27 standarized by JIS corresponds to AISI304 stainless steel.

6. Interaction between Material and CO_2 Laser Beam

(1) Introduction

The absorptance of metal with smooth surface is so low even after melting as described in the last section that more than 85 % of impinged laser beam is reflected out. This makes the CO_2 laser processing of metal inefficient, sometimes even impossible. The absorptance, however, is markedly affected by the surface condition, and thus in order to improve the absorptance a surface treatment was employed.

When a specimen coated with thin layer produced by the surface treatment is heated by high power focused laser beam, condition of this layer in heated region varies with time due to melting, evaporating or spattering so that the absorptance also varies with time. In general the absorptance is not steady at all, but it should be a function of a heating time as well as power level of the laser beam, optical and thermal proporties of the specimen and its surface treatment.

In this section, transient absorptance and temperature of specimen are measured, and a interaction between focused CO_2 laser beam and metal specimen with various surface conditions are discussed on the basis of these experimental data and observation by means of a high speed camera. In addition, interaction between CO_2 laser beam and non-metallic material is also discussed.

(2) Interaction between the Focused CO_2 Laser Beam and Metal with Various Surface Conditions

Interaction between the focused CO_2 laser beam and metallic specimen was discussed based on the absorptance, temperature measured or calculated and observation by means of a high speed camera.

Measurement of the beam absorptance was carried out by the method discribed in section 5. A temperature rise at location on the axis of the impinged focused laser beam on the back surface was measured. To make the response time of measurement fast, a fine Chromel wire, 0.1 mm in diameter, was welded to its back surface by means of condenser-discharge type of spot welder, and potential difference generated between the Chromel wire and the specimen was recorded by an oscillograph.

Transient temperatures of specimen on the axis of the laser beam on the top and back surfaces were computed from Eq. (10). In this computation, informations on energy distribution in focused beam spot, the laser output waveform and transient beam absorptance of the specimen are necessary. The measured energy distribution and the output waveform are shown in Fig. 7 and **Photo. 1** respectively. For the transient beam absorptance, the experimental data obtained in this section were used.

The interaction is discussed by using mainly two kinds of metals with different physical constants, SUS27 stainless steel and aluminum.

Many surface treatments were examined and a series of tests was carried out to evaluate their effect on the absorptance. Surface conditions employed are divided into three groups according to their absorptance characteristics:
(a) roughened, (b) corted with non-metallic thin film and (c) coated with fine metallic and non-metallic powder.

(a) Surface-roughened specimen

In order to analyze the relation between the surface roughness of the specimen and the absorptance, the specimen was roughened with sand papers having various grain size. This treatment is practical and wide range of roughness is easily obtained with reproducible properties. The absorptance was measured after the roughened specimen was rinsed with benzen.

In **Figs. 16** and **17** the absorptance is plotted vs the roughness in term of the number of the sand paper. The relation between the abrasive grain size of the sand paper and its number[4] is listed in **Table 1.**

Table 1. Relation between the abrasive grain size and number of sand paper.

number	240	280	320	400	500
abrasive grain size (μ)	80	67	57	40	34

As shown in **Fig. 16,** the absorptance at room temperature (open symbols) has a tendency to increase

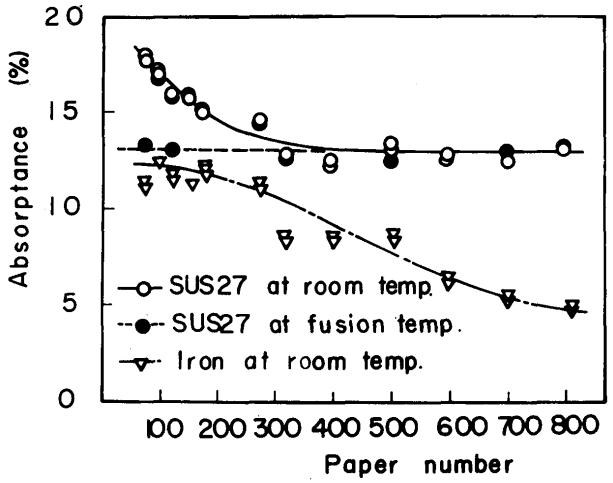

Fig. 16. Absorptance of SUS27 and iron with a surface roughened by a sand paper at room and fusion temperatures.

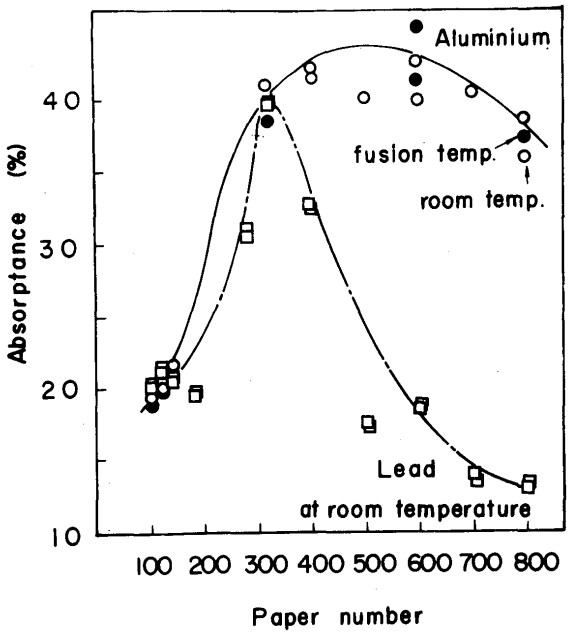

Fig. 17. Absorptance of aluminum and lead with a surface roughened by a sand paper at room and fusion temperatures.

with increasing the surface roughness for iron and SUS27. However, once the surface melts, the absorptance (filled symbols) decreases down to a constant value (for example in case of SUS27, about 13 %) which agrees with the polished one.

On the other hand, as shown in **Fig. 17,** the absorptance curves of both aluminum and lead have apparent maxima at #300～ #500 of roughness region at room temperature. The maximum values are considerably larger than polished; 45 % for Al, which is larger by nearly a factor of 20 than the polished, and 40 % for Pb, which is larger by a factor of 4–5 than polished. Both specimens treated with sand paper appeared to be blackened, especially at maxima of the absorptance curves. These phenomena did not occur for iron and SUS27. The increasing in the absorptance of both Al and Pb seems to be caused by the fine particles of the sand paper attached on their soft roughened surface rather than by roughening or to be oxidized. Namely, the high absorptance measured at room temperature is maintained after melting because the fine particles or oxidized film remain on the surface, whereas the effect of the roughening alone is lost on melting as shown in SUS27.

It was found that the surface treatment with sand paper gives the high absorptance for both Al and Pb, after all, thought the roughening treatment leaves the fine sand particles or oxidized film on their base surface. This treatment, however, seems to belong to the category of the treatment of coating with non-metallic films rather than that of the surface roughening.

(b) Specimen coated with non-metallic thin film

The Fe_2S_3 and Al_2O_3 films were formed on the SUS27 stainless steel and aluminum specimens with 0.3 mm in thickness by the sulphurizing and anodizing respectively. These films had sufficient uniformity and reproducible properties. The absorptance of the SUS27 specimen increased with sulphurizing time, but it reached a constance value, about 80 %, at 7 minutes (110°C) and did not increase any more.

On the other hand, the anodized film produced in dilute sulphuric acid can grow up to sufficient thickness providing 100 % absorptance at room temperature because of its porous structure. Anodizing was carried out in a 15 % solution of H_2SO_4 at a temperature of 20°C and anode current was 1.2 A/dm^2.

(b—1) SUS27 stainless steel specimen

In **Fig. 18** absorbed energy is plotted as a function of beaming time for SUS27 coated with Fe_2S_3 film with 150 W focused laser power. A solid curve shows the absorptance computed by differentiating the absorbed energy curve with respect to time. The absorptance obtained from the temperature measurement, which is shown by open circle symbols in this figure, agrees with solid curve precisely. This absorptance curve decreases rapidly with time at first, and then its decreasing rate becomes gradual. The

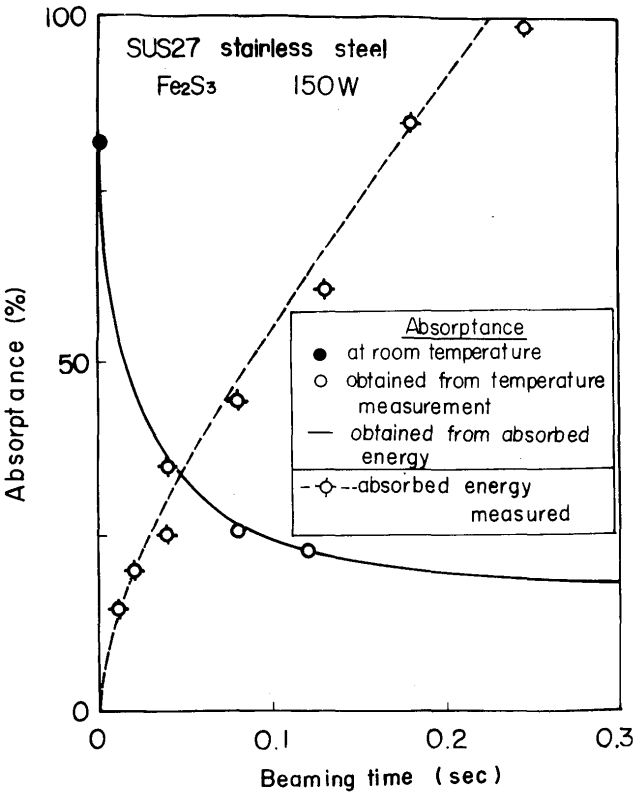

Fig. 18. Relationship between absorptance and beaming time for sulpherized SUS27 stainless steel of 0.3 mm thickness.

absorptance seems to fall down to that of polished, about 13 %. These results show that the decrease in absorptance is due to removal of Fe_2S_3 film via evaporation.

Both top and bottom surface temperature rises at location on the beam axis were computed based on this result shown in **Fig. 19.** **Figure 20** shows measured temperature rises of sulphurized and

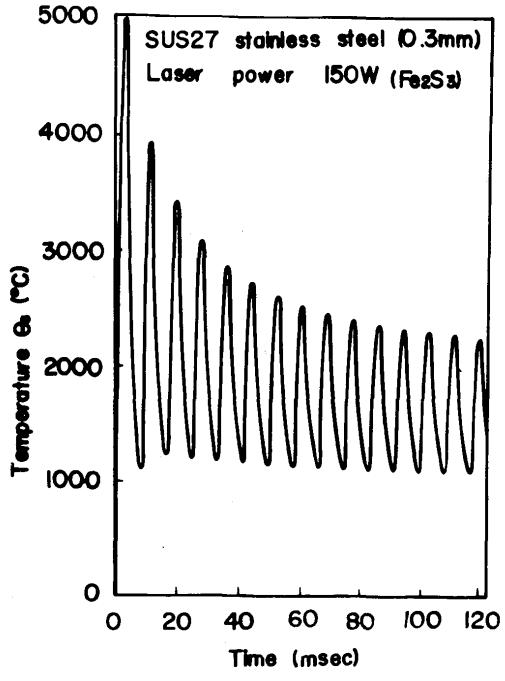

Fig. 19. Calculated temperature rise at top and bottom surface of 0.3 mm thick SUS27 at location on the beam axis. Characteristic curve of the absorptance is shown in Fig.
(a) at top surface. (b) at bottom surface

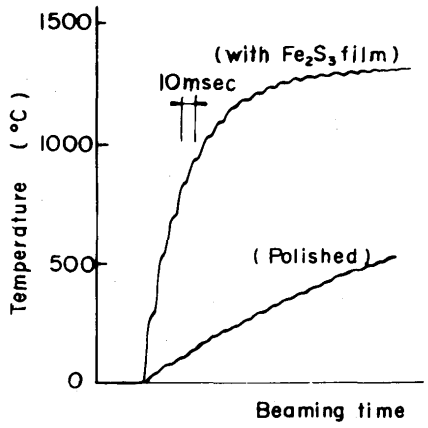

Fig. 20. Temperature records of the sulpherized SUS27 of 0.3 mm thickness at bottom surface on the beam axis (laser power = 150 W).

polished 0.3 mm SUS27 under the same condition. Experimental values in both polished and sulphurized agree well with the theoretical results. The theoretical top surface temperature varies violently with time according to the laser power output waveform with a period of 1/120 sec, having maximum of temperature for each pulse. Though a maximum temperature corresponding to the first pulse is the highest, after that the maximum temperatures decrease sharply with time in spite of condinuous heating because of decrease in the absorptance. In the first and second pulses, it is clear that the surface temperatur becomes enough high for Fe_2S_3 film to evaporate, and thereafter the surface temperature is also enough high. Thus it was confirmed from the theoretical analysis of the temperature rise that Fe_2S_3 film cannot remain on the base metal so that the absorptance decreases down to the value in the polished surface condition, infferred from Fig. 18.

Photograph 2 shows the high speed photographs of the surface condition during laser heating. In the first pulse an evaporation is clearly observed, in the second pulse it becomes relatively weaker and thereafter it may be no longer observed. But in the third pulse and after, a weak evaporation seems to continue. These observation agrees with the tendency infered from the analysis of temperature rise described above.

On the other hand, there was little fluctuation in computed temperature curve of 0.3 mm sulphurized SUS27 at the bottom surface at location on the beam axis. Its temperature is elevated sharply within initial 5–10 pulses and subsequently it does not almost increase. The temperature rise corresponding to polished one (A_f=13 %) is also shown in this figure. The temperature of polished specimen is elevated very slowly in comparison with the sulphurized one.

In the case CO_2 laser is applied to the welding of

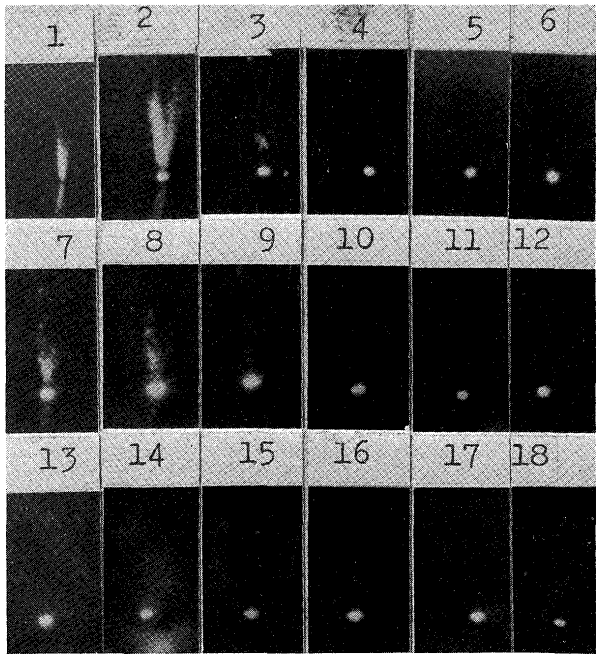

Photo. 2. Highspeed motion pictures of sulpherized SUS27 of 0.3 mm thickness heated by focused laser beam with power 150 W (700 frames/sec). 1～6 correspond to the first pulse, 7～12 the second pulse and 13～18 the third pulse.

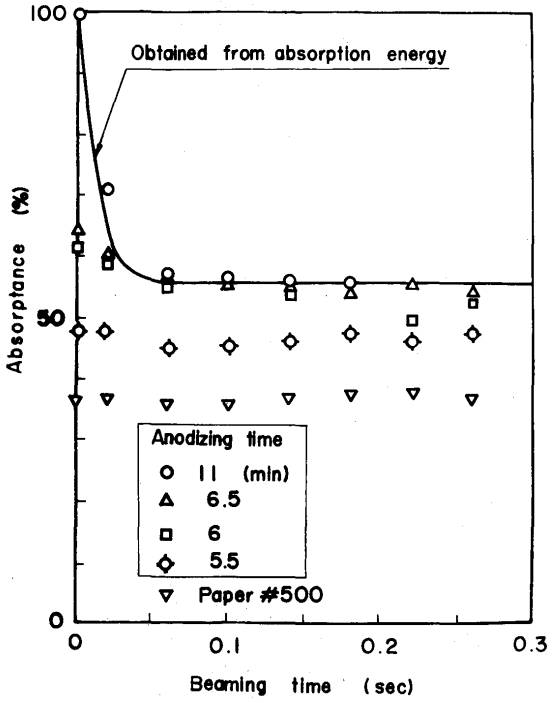

Fig. 21. Relation between absorptance and beaming time for anodized Al of 0.3 mm thickness.

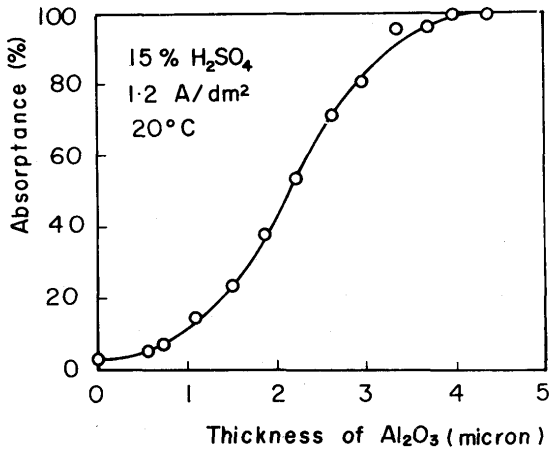

Fig. 22. Thickness of Al_2O_3 vs the absorptance at room temperature.

SUS27, in order to obtain full penetration the response time of temperature rise at bottom surface is fairly long due to its poor thermal diffusivity. Therefore a situation under high beam absorptance must be maintained for a long time. This means that surface layer must remain on the base metal for a long time. But in order to melt the bottom surface, it is inevitable that temperature at the top surface becomes so high that the surface layer evaporates away as the temperature gradient within the base metal in the direction of the thickness becomes large due to its poor thermal diffusivity.

From the consideration based on the heat conduction theory, one can make the following statement: in order to enhance the absorptance, it is necessary for the thin surface layer to remain at the top surface of base metal under high temperature condition.

(b—2) Aluminum specimen

Figure 21 shows the change of the absorptance with time when focused laser beam with power level of 150 W impinged upon 0.3 mm Al specimens coated with Al_2O_3 films taking the anodizing times; 11, 6.5, 6 and 5.5 minutes. They have 100, 64, 61 and 48 % absorptance respectively at room temperature. The relation between the absorptance and the thickness of Al_2O_3 film is plotted in **Fig. 22.** As shown in Fig. 21, the absorptance decreased sharply down to constant value, about 55 %, though it was much higher than 3.7 % for polished, during initial 50 msec of beaming time for the three specimens corresponding to 100, 64 and 61 % absorptance at room temperature. It does not, however, change for the specimen corresponding to 48 % absorptance at room temperature.

These results show that Al_2O_3 film with thickness corresponding to 55 % absorptance at room temperature can still remain on the 0.3 mm Al specimens when 150 W-focused laser beam impinges upon the specimen. According to Fig. 22, which shows relationship between thickness of Al_2O_3 and absorptance at room temperature, it is estimated that Al_2O_3 film having 2.2 μ in thickness can remain.

In order to confirm thes results, specimens were weighed both before and after the irradiation of 150 W-focused laser beam under the same condition. Since the decrease in weight is very small, long bead,

30 cm long, was formed. The decreased weight, in mg is plotted as a function of the absorptance at room temperature in **Fig. 23.** There were almost no

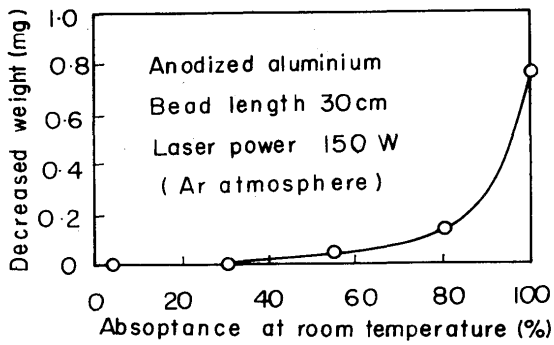

Fig. 23. Relationship between the absorptance of anodized Al at room temperature and the decreased weight for bead length 30 cm.

decrease in weight for specimens having lower absorptance than 55 % at room temperature, though appreciable decrease occured for the specimen having the higher absorptance than 55 %.

The computation of the residual thickness was made for the specimen having the 100 % absorptance at room temperature under the following assumptions: (1) Al_2O_3 film has a density of 2.5 g/cm^3 [5] (2) The film is removed in the rectangular shape of 0.5 mm wide by 30 cm long with a certain uniform thickness. (3) The film has an uniform thickness of 4 μ before laser heating. (4) The residual film is of uniform thickness and its density does not change after melting.

Since the computed thickness of removed Al_2O_3 film was about 2 μ, the thickness of the residual film was equal to 2 μ, which was in good agreement with the thickness (2.2 μ) corresponding to the constant absorptance (55 %) in Fig. 22. It was verified that the decrease in the absorptance of anodized Al was due to removal of the Al_2O_3 film via evaporation, and that a certain thickness of the film remains so as to keep considerably higher absorptance.

This constant value, to which the absorptance of such an anodized Al falls, decreases with increasing the focused laser power as shown in **Fig. 24,** because the amount of Al_2O_3 film removed due to evaporation increases with increasing the laser power.

Namely, during laser heating it seems that the top surface of the Al_2O_3 film will reach its boiling point or above, and that the bottom surface, which contacts with the top surface of the aluminum sheet, should have the same temperature as the aluminum top surface having the considerably lower temperature in comparison with that of top surface of the film. Therefore the steep gradient in temperature should be produced within the film in the direction of

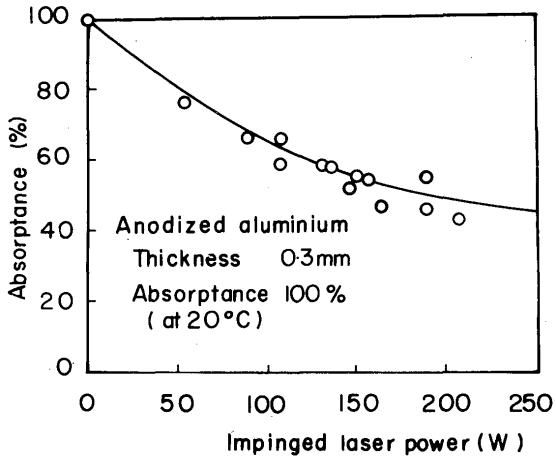

Fig. 24. Impinged laser power vs absorptance of anodized aluminum of 0.3 mm in thickness for steady heating.

the thickness, and thus a part of film heated over its boiling point is removed.

Such an inference will be verified by inquiring the temperature of the specimen as follows.

Figure 25 shows the computed temperature rises of anodized 0.3 mm Al sheet on the beam axis. It was assumed that the anodized Al had 100 % absorptance at room temperature and that its transient absorptance curve was given by Fig. 21. In the same manner as the SUS27 specimen, at the top surface the temperature rise in the first pulse is the highest. However, it shoud be noticed that the surface temperature of the base metal is low, 1600°C at the highest, which is considerably lower than the boiling point of Al_2O_3 coated on the base metal. Therefore the Al_2O_3 film can remain even after the anodized specimen is heated and melted by focused laser beam for a long time, and enhances the beam absorptance.

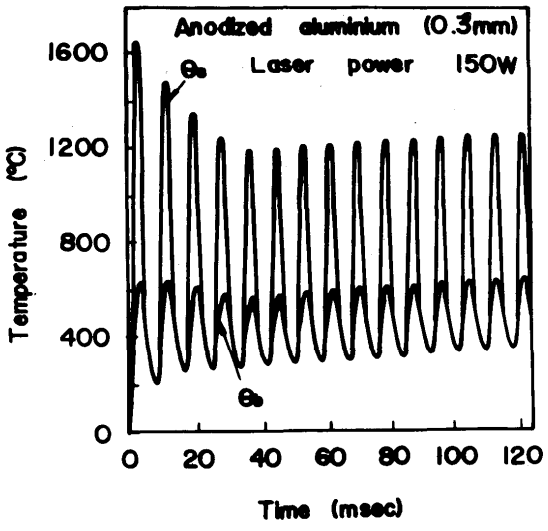

Fig. 25. Calculated temperature rise on the beam axis (r=0) of anodized aluminum, 0.3 mm in thickness. Transient absorptance is shown in Fig. 21, and θ_s and θ_b correspond to the temperature rise at top and bottom surfaces.

The bottom temperature also becomes the highest during the first pulse. It can be assumed from computation that both melting and solidification of specimen at both top and bottom surface occur in each pulse duration because of its high thermal diffusivity. High speed motion pictures were taken to confirm the computed results. As shown in **Photo. 3** which is experimented under the same condition as the computation, indicates that results on the basis of observation agree qualitatively with computed.

When anodized 0.3 mm Al specimen was heated by focused laser beam, its bottom temperature at location on the beam axis was recorded as shown in **Fig. 26.** The absorptance of the specimen used was 100 % at room temperature and the laser beam impinged at same location four times. In this case each beaming time (150 W) was 200 msec. The absorptance corresponding to the first heating with time duration of 200 msec is assumed to vary according to a solid curve shown in Fig. 21: at the end of the heating period, the absorptance is already constant value, 55 %, and thereafter further heating, which involves

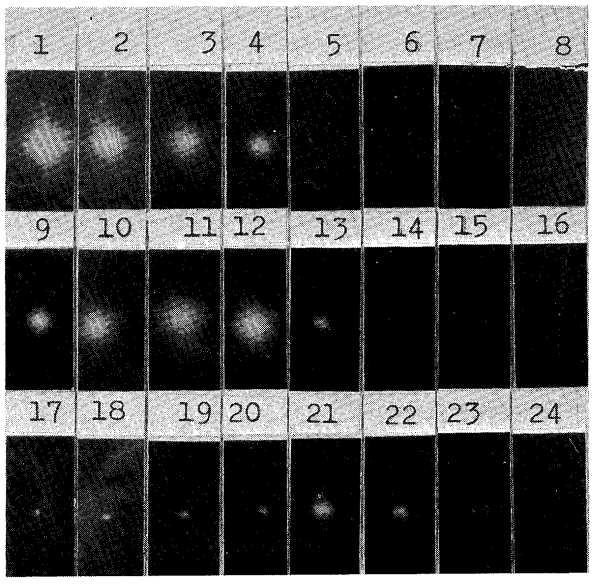

Photo. 3. High speed motion pictures of anodized aluminum of 0.3 mm thickness heated by focused laser beam with power 150 W (1000 frames/sec). 1～8 correspond to the first pulse, 9～16 the second pulse and 17～24 the third pulse.

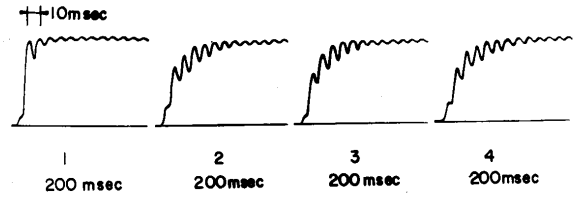

Fig. 26. Temperature records of anodized aluminum of 0.3 mm in thickness at location on the beam axis of bottom surface.

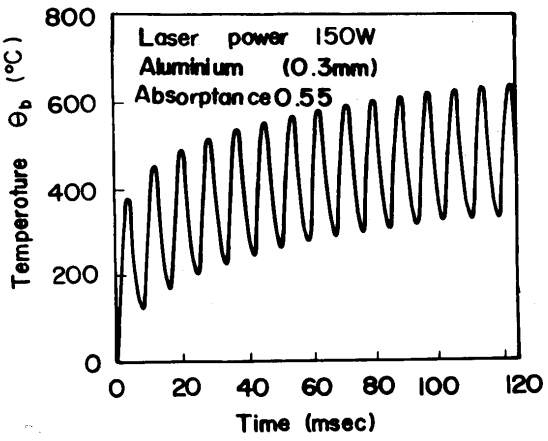

Fig. 27. Calculated temperature rise of aluminum, 0.3 mm in thickness with constant absorptance 55 % at location on the axis of bottom surface.

the second, third and fourth heating, does not change the absorptance. Actual temperature measurements confirm that the constant absorptance value is kept from the second heating. **Figure 27** shows behavior of the calculated temperature corresponding to the experimental results indicated in Fig. 26 (b), (c) and (d). The computed results corresponding to Fig. 27 (a) is shown in Fig. 25. Both experimental and computed results are qualitativery in good agreement. Comparison between Fig. 19 (a) and Fig. 25 or Fig. 19 (b) and Fig. 27 shows how fast the bottom surface temperature of Al responses in comparison with SUS27.

It was found that the absorption proporties of anodized Al was quite distinct from that of sulphurized SUS27, i. e. the film in the former remained and contributed to enhance the absorptance, but in the latter did not remain at all when focused laser beam impinged upon the specimen for relatively long time. Since the films bottom surface has the same temperature as the top surface of the base metal as described already, whether the film remains or not at the surface depends on the surface temperature of the base metal and the boiling point of the film. In the case of Al, its surface temperature is not so high because of its high heat conductivity, keeping the temperature of the film's bottom surface (contacted to the base metal) lower than its boiling point, for the given focused laser power. On the other hand, in the case of SUS27 the top surface temperature of the base metal may exceed the boiling point of the surface-treated film due to the low heat conductivity.

(c) Specimen coated with non-metallic fine powder

The specimen coated with non-metallic fine powder had neary 100 % absorptance at room temperature. Fine powder (>200 mesh), here a flux of the submerged welding was used, dissolved with proper

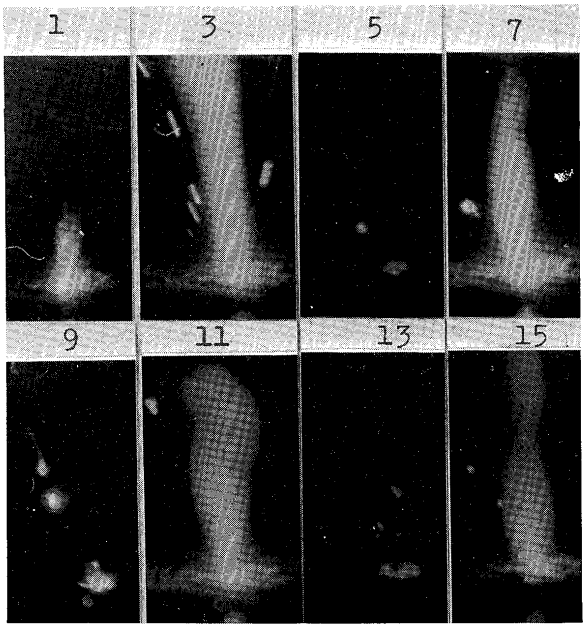

Photo. 4. High speed motion pictures of SUS27 specimen of 0.3 mm thickness coated with non-metallic fine powder (500 frames /sec). 1~3 correspond to the first pulse, 5~7 the second pulse, 9~11 the third pulse and 13~15 the fourth pulse.

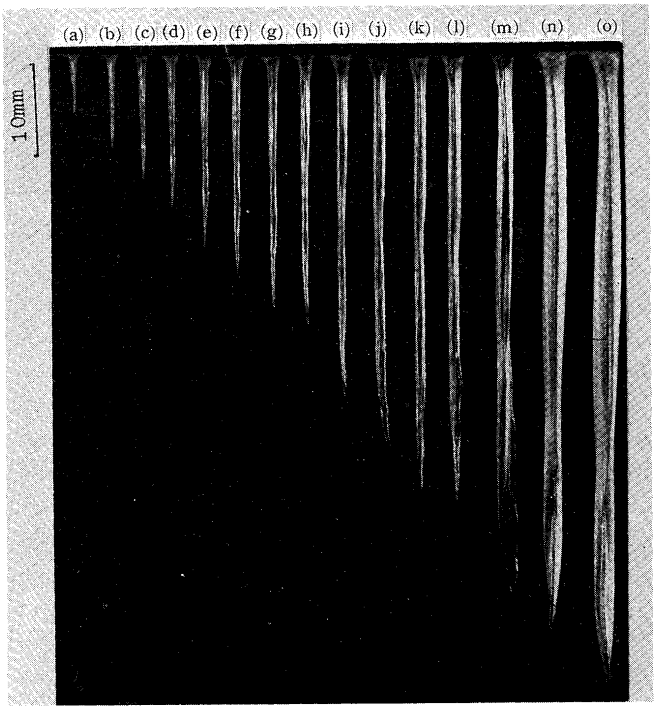

Photo. 5. Acrylic resin drilled by laser beam with power 360 W. Irradiation time (sec):
(a) 0.02, (b) 0.04, (c) 0.06, (d) 0.08, (e) 0.13, (f) 0.18, (g) 0.23, (h) 0.28, (i) 0.28×2, (j) 0.28×3, (k) 0.28×4, (l) 0.28×5, (m) 0.28×10, (n) 3.0, (o) 5.0.

concentration in alcohol was spread on the surface of metal so as to form an uniform layer, and then was dried in the air. The best result was obtained when the density of the coated layer was 30 mg/cm^2. **Photograph 4** shows high speed motion pictures of non-metallic fine powder. In the first pulse, distinct evaporation as well as spattering of the surface layer is observed and evaporation is still continued for longer time than the case of Fe_2S_3 film coating. While the evaporation continuous, it seems that the surface layer attaches closely to the base metal in the form of thin film as a result of its melting, and enhances the absorptance. From the consideration based on the heat conduction theory, in order to enhance the absorptance, it is necessary for thin layer to remain at the surface of the specimen under even high temperature condition. Based on this inference, specimen coated with non-metallic fine powder may have higher absorptance than one coated with Fe_2S_3 film.

(3) Wall-Focusing Effect

Since the laser beam focused by an optical system is not parallel but has an appreciably large convergent angle, it is natural to inquire whether a laser processing of thick material is possible or not. In this section several examples of laser precessed materials are illustrated, and feature and possibility of laser processing of thick material are disucssed on the basis of these results.

Photograph 5 shows an example of the laser-drilled acryl for various beaming times. In this experiment the laser beam with the power level of about 360 W was focused just upon the acryl. The holes were slender and nearly cylindrical in shape, and always had a wedge shape top with a very acute angle even at for off-focal point as shown in Photo. 5.

In most case the diameter of the hole which was somewhat larger at the top surface varied with the depth having a peak value at two locations. From these facts, drilling mechanism by the focused laser beam can be shown as follows; At first, incident laser beam drills a hole with small diameter. As the following beam incomes the hole with very large incident angle with the well of the hole, near 90°, it reflects with almost 100 % reflectance.

Then the reflected beam will be re-focused at the bottom edge as shown shcematically in **Fig. 28** giving

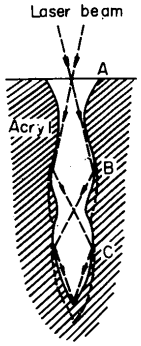

Fig. 28. Wall-focusing action in the hole drilled by the lase beam.

acute edge angle at bottom of the hole. The authors named this phenomenon as "wall-focusing effect" of the laser beam. From Fig. 28 the incident beam seems to be reflected about two times to reach the bottom eadge by the wall of the hole resulting in two peak portions of the hole diameter at B and C, because the wall of the drilled hole which is not completely smooth, absorbs the beam energy much larger at main reflected points (B and C) than other part.

To confirm the wall-focusing effect of the laser beam, two acryl plates of 5 mm in thickness were heated by the focused laser beam with different distances between two plates. In this test, the beam was focused on the top surface of the upper plate. The shape of the drilled holes is shown in **Photo. 6.** When the distance d was zero, the beam diameter at the bottom surface of the upper plate, ϕ_{1b}, was same as that at the top surface of the lower plate, ϕ_{2t}. The remarkable features in case of $d \neq 0$ were that a discrepancy between ϕ_{1b} and ϕ_{2t} increasing the distance d and the hole of the lower plate became quasi-conical in shape. From d-value and the difference between ϕ_{1b} and ϕ_{2t}, divergent angle about 5° of the beam passed through the hole of the upper plate was obtained. It is, however, noteworthy that the beam diameter at bottom surface of the lower plate, ϕ_{2b}, was considerably smaller than that of the upper plate (ϕ_{1b}). It is clear from these facts that the beam is re-focused inside the laser-drilled hole, namely the wall-focusing effect exists in laser drilling, and the effect is not available without surrounding wall. In general, such the wall-focusing phenomenon of the high power laser beam should occur in heating of any material involving solid and liquid if the heating was accompanied by the drilling action. Since the drilling action becomes remarkable as the laser beam power and its density increase, the wall-focusing action depends upon the beam power and its density. Therefore the wall-focusing action becomes effective in the material having low thermal conductivity, easily sublimated or vaporized property and small latent heat of the

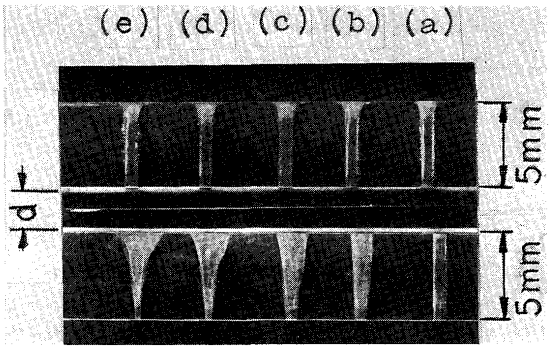

Photo. 6. Shape of drilled hole of acrylic regin with various distance d. Distance d(mm): (a) 0, (b) 3, (c) 6, (d) 9, (e) 12.

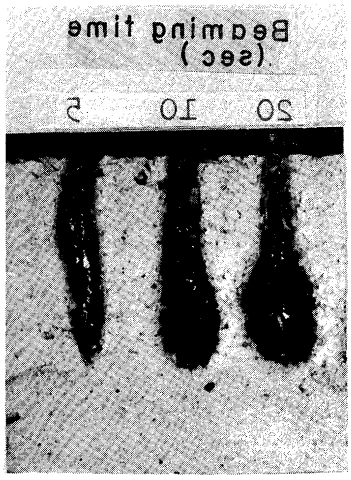

Photo. 7. Laser drilled firebrick (lase power= 250 W) Irradiation time (sec): (a) 5, (b) 10, (c) 20.

vaporization of the sublimation such as acryl. **Photograph 7** indicates the cross section of the laser drilled firebrick. In this case until the beaming time was about 5 sec, the bottom edge of the drilled hole possesed an actute angle due to the wall-focusing action. And then the depth of the hole reached the limit and did not increase any more. Such limiting depth depends upon the beam, focusing condition, beam power and material. After reaching the limiting depth at which the vaporization was supressed or stopped, the bottom wedge shape of the hole become gradually round shape so that the wall-focusing action disappeared.

As described above, the wall-focusing action occured also for liquid material. **Photograph 8** illustrates the wall-focusing action for water. In this case the bottom edge was somewhat round in comparison with above two examples. This is due to both surface tension and vaporized pressure of the water.

In case of metal, the wall-focusing phenomenon should also take place in higher laser beam power

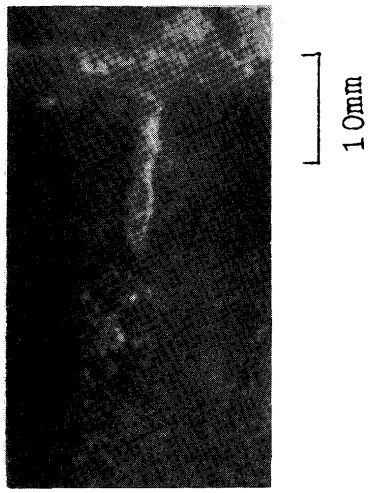

Photo. 8. Laser drilled water (laser power=250 W).

which induced the drilling action. From these results it can be predicted that so called "deep penetration" which has been typical in electron beam welding only is also obtained in high power laser beam welding. Consequently it was clarified that laser beam processing involving deep penetration welding, cutting and drilling of thick material, also became possible as well as electron beam heat source by introducing the new developed idea, wall-focusing effect of the laser beam.

7. Laser Processing

(a) Welding

In laser processing such as but-welding of thin metal, it is necessary to obtain the absorption characteristics of moving specimen or moving laser spot. A series of bead-on-plate tests were carried out on both anodized Al and sulphurized SUS27, and the absorptance was measured as a function of the traveling velocity of the laser heat source and the laser power level, using the calorimeter.

Figure 29 shows examples of relation between the traveling velocity and the absorptance. In general, the absorptance of the metal specimen coated with non-metallic films was inclined to increase with increasing traveling velocity.

Figure 30 shows examples of relation between the

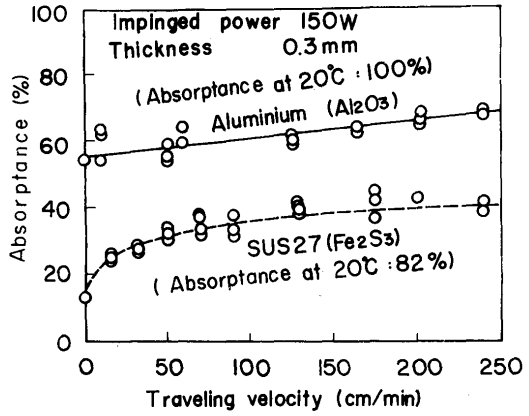

Fig. 29. Effect of impinged laser power on the absorptance at constant traveling velocity.

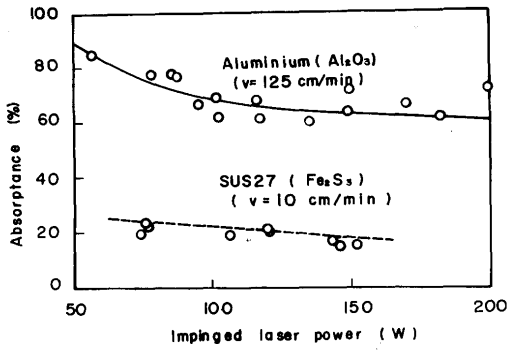

Fig. 30. Effect of traveling velocity on the absorptance at constant laser power.

impinged laser power and the absorptance at given constant traveling velocities. The absorptance had a tendency to decrease with increasing laser power because of the remarkable removal of the films owing to the evaporation.

The effect of surface treatment on the absorptance of Al was higher than that of SUS27 as shown both in Figs. 29 and 30, though Al had much lower absorptance than SUS27 under polished surface condition.

When the film coated on the metal surface had very low boiling point in comparison with base metal, the effect of the film on the absorptance could not be expected. Although the specimen coated with a paint had nearly 100 % of absorptance at room temperature, at the moment the focused laser beam impinged upon the specimen, the paint film evaporated completely, and had little effect on the absorptance.

The same tendencies were observed in other surface treatments. In general, the decreasing rate of the absorptance with increasing laser power was higher for surface layer material with lower boiling point and for the base metal with lower thermal conductivity and higher melting point. These may be expected from the facts described in section 6.

In order to study the effect of the surface treatment on the welds, concentration measurement of the element involved in the surface-treated layer and and mechanical test were made. Distribution of the concentration in the weld bead was measured for a laser-heated SUS27 stainless steel specimen coated with non-metallic fine powder. **Figure 31** shows the silicon content which is the principal constituent of the non-metallic fine powder. Silicon content was neglible in molten metal. Non-metallic powder seems to vaporize away and have no bad effect on the bead. Similar results were obtained from other kinds of surface treatment.

Tensile test transverse to the direction of butt welding was made for SUS27 stainless steel specimen. The surface conditions used were (1) polished, (2) coated with metallic fine powder, (3) coated with non-metallic fine powder, and (4) sulphurized. Test specimens failed usually in the base metal or heat affected zone in the cases of surface conditions (1) and (2),

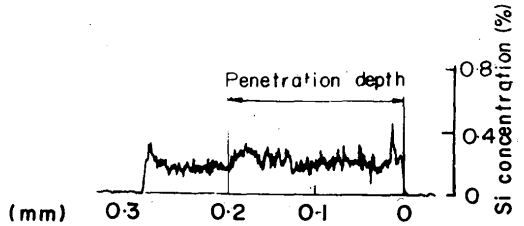

Fig. 31. Distribution of Si concentration in SUS27, 0.3 mm in thickness, coated with non-metallic fine powder, measured in the direction to the thickness.

and sometimes in the weld bead in (3) and (4). There were, however, almost no difference in tensile strength between both cases, and the weld joint efficiency ranged from 90～100 %.

When a V-shaped joint is irradiated by the laser beam, the incident beam is effectively trapped in the V-shaped groove.

Photograph 9 shows an example of V-joint weld as a result of improving the beam absorptance based on this idea. In this case, the absorptance of about 60 % was measured. Such a condition having high beam absorptance may be also realized by the drilling action of the high power laser beam as described above. But the depth of the drilled hole and the thickness of weld are limited by the laser power. In case of V-joint welding, there are no limiting thickness in principle.

In order to compare the effect of each surface treatment on the absorptance under same condition, a full penetration power for various metals with a given thickness was measured under various surface conditions.

The data for 0.3 mm SUS27 are shown in **Fig. 32.** There was little difference between polished specimen and one coated with paint: a film made of material of low boiling point such as paint had little effect on the absorptance. There was considerably larger difference of the effect of the absorptance in the surface treatments. Coating with non-metallic fine powder was the most efficient surface treatment among the others as infered in the last section. On the other hand, coating with metallic fine powder had not so large effect as non-metallic fine powder, because once metallic powder melted it acted as a polished metal. But since non-metallic fine powder melted to form the

Photo. 9. Cross section of V-joint weld (0.3 mm thick SUS27).

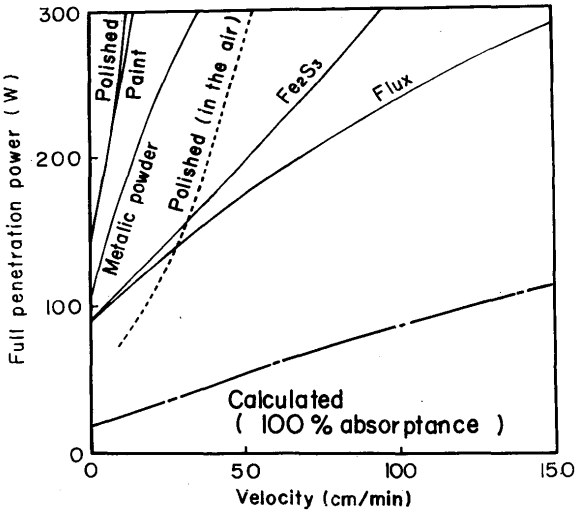

Fig. 32. Full penetration power for SUS27, 0.3 mm in thickness, with various surface conditions.

non-metallic thin film, it had high absorptance even after melting.

The data for aluminum, 0.3 mm in thick, are shown in **Fig. 33.** Under polished surface condition, even the surface of the specimen did not melt with power level of laser beam used in this experiment because of its extremely high reflectance. The absorptance was remarkably improved by the surface treatments, and there were only a little difference of the effect on the absorptance in the surface treatments in the case of Al. At low speed, difference between calculated and experimental values is very small, as if the absorptance values were very high. This is because the test piece had not infnite width.

It should be noted that coating treatment with aluminum fine powder had nearly the same effect as non-metallic fine powder in contrast to the case of SUS27. It is believed that full penetration of Al specimen may be obtained at the moment when the layer of Al fine powder, which has high absorptance only at solid state, melts down, due to its high thermal

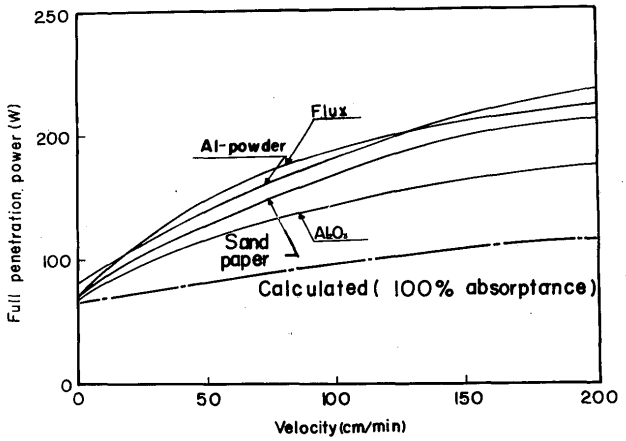

Fig. 33. Full penetration power for aluminum, 0.3 mm in thickness, with various surface conditions.

conductivity and small thickness, 0.3 mm. Specimen coated with paint film, of which data are not indicated in this figure, does not melt even at the surface, because the paint evaporates easily since its boiling point is much lower than the base metal.

(2) Cutting

High speed fine cutting of sheet steel with narrow kerf width and heat affected zone has been accomplished which employs a focused laser beam for preheating in combination with an oxygen jet. This new cutting method, combined laser energy and chemical reaction energy such as an oxidation energy, it names as "laser gas cutting method" in distinction from laser cutting method which employs laser alone.

The distance between the oxygen nozzle and work piece was 1.5～2 mm. The quality of cut of laser gas cutting has been estimated based on the roughness of the cutting edge h: the cut with $h<$ 0.05 mm is classified to a fine cut and the cut with $h>0.05$ mm rough cut. **Figure 34** shows the quality of cut (SS41) with various thickness as a function of the laser power. **Figure 35** shows the influence of

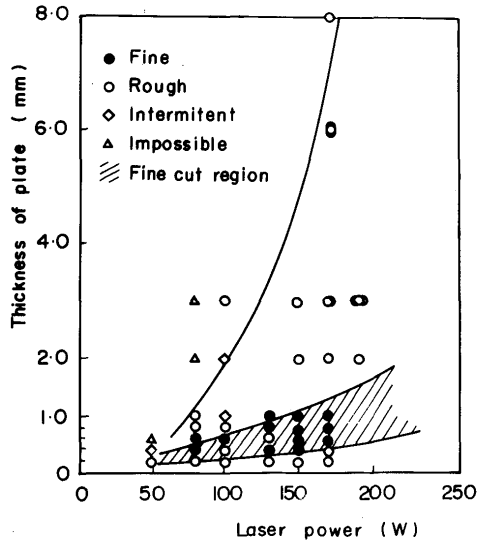

Fig. 34. Quality of cut with various thick plate (SS41) as a function of laser power.

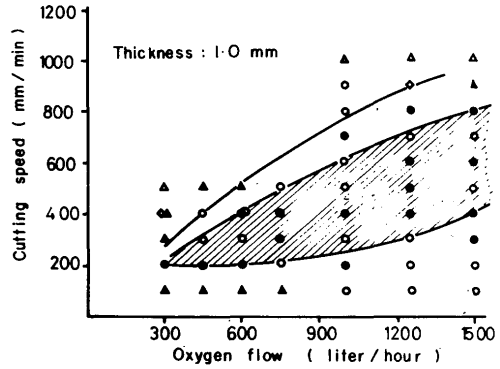

Fig. 35. Relationship between quality of cut and cutting conditions.

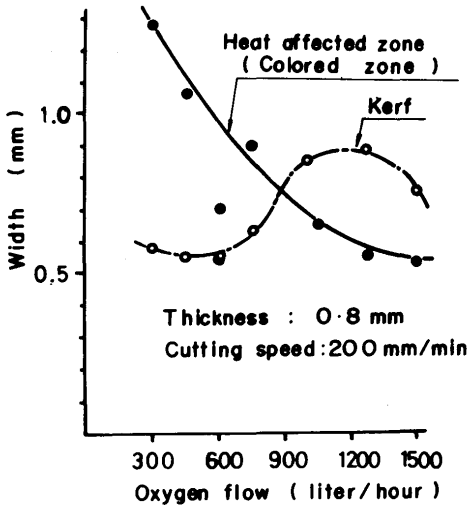

Fig. 36. Kerf width vs oxygen flow.

the cutting speed and oxygen flow on the quality of cut. If the laser power is too high, molten slag tends to freeze out on the cutting edge providing a rough cut and wide kerf. **Figure 36** shows an influence of cutting speed on the width of the kerf and the colored zone. The narrowest kerf width of 0.5 mm, which corresponds to the diameter of beam spot, was obtained.

8. Conclusion

In welding metal by CO_2 laser with power level of several hundred watts, one of the most serious probrems is that the beam absorptance of metallic surface is extremely low.

This paper discusses the interaction between the focused laser beam and metallic specimen with various surface conditions based on measurements of the beam absorptance and the temperature, observation by means of high speed camera and analysis of heat conduction.

The radial energy density distribution profile of the laser beam in the focal spot was approximated by a Gaussian curve with the diameter 0.5 mm at e^{-1} power point; which was about four times that of coherent beam.

The absorptance of sheet metal obtained from the commercial vender was almost proportional to the square root of dc electrical resistivity at both room and fusion temperatures.

A weldability, which was calculated based on optical and thermal properties of metal, was proportional to $ak^{3/2}\theta_f$ under the pollished surface condition, and to $ak\theta_f$ under the condition of 100% absorptance. The effect of the surface treatment on the beam absorptance become larger with lower melting point θ_f of and higher thermal conductivity k of the metal and

higher boiling point of the treated surface layer, and under such a condition the absorptace was almost same in different surface treatments.

References

1) Y. Arata, I. Miyamoto and M. Kubota: I.I.W. Doc. IV-4-69 (1969).
2) D. Rosenthal: Mathematical Theory of Heat Distribution during Welding and Cutting, W. J. Vol. 20 (1941), No. 5, 220s–234s.
3) E. Hagen and H. Rubens: Ann. Physik, Vol. 11 (1903), 873.
Electron Theory of the Optical Properties of Metals for Silver, Gold and Copper in the Near Infrared, JOSA, Vol. 44 (1954), No. 7 504-545.
H. E. Bennett, M. Silver and E. J. Ashley: J. Opt. Soc. Am. Vol. 53 (1963), 1089.
J. M. Bennett and E. J. Ashley: Infrared Refrectance and Emittance of Gold Evaporated in Ultrahigh Vacuum, Appl. Optics Vol. 4 (1965), No. 2, 221-224.
4) JIS R6252-1966 Abrasive paper.
5) Aluminum Tashenbuch, 12, Anflage S. 576.